Dissipation phenomena and magnetic phase diagram of Cu_2OSeO_3 below 50 K

F. Qian,[1] H. Wilhelm,[2] A. Aqeel,[3] T.T.M. Palstra,[3,†] A.J.E. Lefering,[1] E.H. Brück,[1] and C. Pappas[1]

[1] *Faculty of Applied Sciences, Delft University of Technology, Mekelweg 15, 2629 JB Delft, The Netherlands*
[2] *Diamond Light Source Ltd., Chilton, Didcot, Oxfordshire, OX11 0DE, United Kingdom*
[3] *Zernike Institute for Advanced Materials, University of Groningen, Nijenborgh 4, 9747 AG Groningen, The Netherlands*

(Dated: November 21, 2016 susc-lowT_cuse.pdf)

The magnetic phase diagram of the chiral magnet Cu_2OSeO_3 has been investigated by dc magnetisation and ac susceptibility over a very large frequency range from 0.1 Hz up to 1 kHz and temperatures below 50 K. Qualitatively different phase diagrams have been obtained by applying the magnetic field along the easy $\langle 100\rangle$ or the hard $\langle 110\rangle$ crystallographic directions. Strong χ'' appears close to B_{c2}, but only below 30 K and is more pronounced when B is applied along $\langle 100\rangle$. In addition, the transition from the helical to the conical phase leads to two adjacent B_{c1} lines below 50 K. The frequency dependence of χ'' indicates the existence of very broad distributions of relaxation times both at B_{c1} and B_{c2}. The associated very long characteristic times eventually prevent the system from reaching thermal equilibrium at low temperatures and lead to thermal hysteresis.

arXiv:1611.06014v1 [cond-mat.str-el] 18 Nov 2016

I. INTRODUCTION

Magnetic chirality generated by the anti-symmetric Dzyaloshinskii-Moriya (DM) interaction is at the focus of interest since the observation of stable skyrmion lattice textures in systems of the B20 family, such as MnSi[1,2], $Fe_{1-x}Co_xSi$[3,4] or FeGe[5,6]. The existence of these particle-like objects in chiral magnets was predicted in the late 1980's by Bogdanov and Yablonskii[7,8] and their topological robustness is at the origin of several new phenomena paving the way to potential applications in data storage and manipulation devices[9].

The multiferroic insulator Cu_2OSeO_3 is a chiral magnet hosting skyrmions, that can be manipulated by electric fields[10,11]. This system has a similar phase diagram as the metallic B20 compounds, determined experimentally by several studies[11–18] close to $T_c = 58.2$ K. At zero field, the helix has a pitch of ∼60 nm arising from the balance between the strongest ferromagnetic exchange and the DM interactions and is fixed by a weak magnetocrystalline anisotropy along the $\langle 100\rangle$ crystallographic directions. Relatively weak external magnetic fields exceeding B_{c1} orient the helices along their direction, leading to the conical phase. High enough fields above B_{c2} overcome the DM interactions and induce a field-polarised state. The skyrmion lattice is stabilised at intermediate fields between B_{c1} and B_{c2} in a narrow temperature window just below T_c.

Cu_2OSeO_3 is characterised by a more complex crystal structure than the metallic B20 compounds, although with the same $P2_13$ space group. The unit cell contains 16 Cu^{2+} ions on two different sites, Cu(1) and Cu(2)[19,20], which form tetrahedra composed of three Cu(1) and one Cu(2). In contrast to the B20 metallic chiral magnets, in Cu_2OSeO_3 the superexchange magnetic interactions between the Cu^{2+} spins and the DM interactions can be calculated ab-initio at the atomic level[21–23] providing a direct link between theory and experiment. This approach reveals the existence of weak and strong magnetic bonds and a separation of exchange energy scales beyond the one encountered in the B20 metallic counterparts[24].

In Cu_2OSeO_3 the building blocks of the magnetic structure are the Cu^{2+} tetrahedra, which interact weakly with each other[22,23]. Within the tetrahedra the spin of the single Cu(2) ion is antiparallel to the spins of the three Cu(1) ions, resulting in a total spin of S=1 and a magnetic moment of ∼0.5 μ_B per Cu^{2+} ion. This description is consistent with the quantum mechanical treatment of the S=1/2 spins and has profound implications on the magnetic properties. In particular, the low temperature phase diagram of Cu_2OSeO_3 is qualitatively different when a magnetic field is applied along the easy $\langle 100\rangle$ crystallographic direction or not[22].

In this study we investigate the $B-T$ phase diagram of Cu_2OSeO_3 at temperatures below 50 K by dc magnetisation and ac susceptibility measurements spanning a large frequency range from 0.1 Hz up to 1 kHz. For a comparison with theory the magnetic field has been applied along the easy $\langle 100\rangle$ and the hard $\langle 110\rangle$ crystallographic directions. The B_{c1} transition from the helical to the conical phase splits in two distinct lines below 50 K, which may be related to the two different Cu^{2+} sites. The transition to the field polarised state at B_{c2} is seen not only on the real component of the susceptibility, χ', but also on the imaginary one, χ'', most prominently for $B \parallel \langle 100\rangle$. The weak frequency dependence of χ'' and thermal hysteresis phenomena at both B_{c1} and B_{c2} reflect the existence of long relaxation times with broad distributions. The results are compared with theory, which predicts more dramatic changes with a first order phase transition at B_{c2} for $B \parallel \langle 100\rangle$ and does not account for the two B_{c1} lines observed.

II. EXPERIMENT DETAILS

Two single crystals of Cu_2OSeO_3 with dimensions of $\sim 1\times1\times1$ mm^3 were prepared by chemical vapour transport method[25,26] and their structure was checked by single crystal x-ray diffraction. One sample was oriented

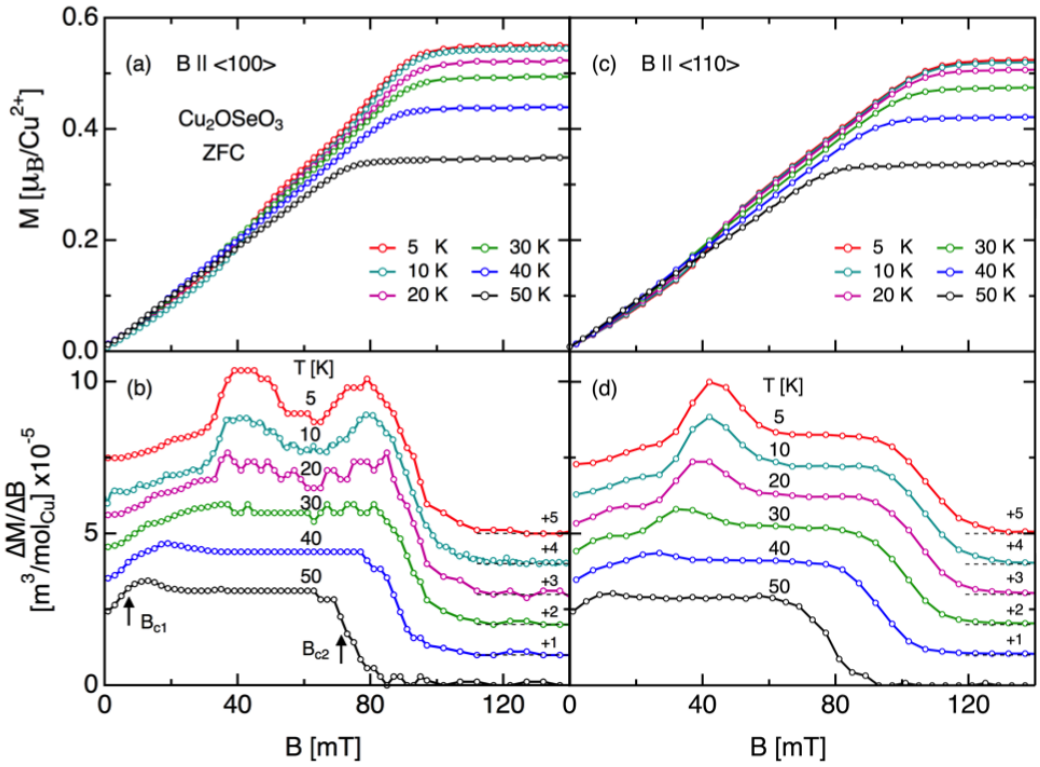

FIG. 1. Magnetic field dependence of the ZFC magnetisation, panels (a) and (c), and of the deduced susceptibility $\Delta M/\Delta B$, panels (b) and (d), of Cu_2OSeO_3 between 5 and 50 K for $B \parallel \langle 100\rangle$, panels (a) and (b), and $B \parallel \langle 110\rangle$, panels (c) and (d). The arrows to the 50 K curve in (b) indicate the critical fields B_{c1} and B_{c2} determined from the inflection points of $\Delta M/\Delta B$. For the sake of clarity the $\Delta M/\Delta B$ curves have been shifted vertically with respect to the base line as indicated.

with $\langle 100\rangle$ vertical and was the same as in the previous study[18]. The other sample was oriented with $\langle 110\rangle$ vertical. The accuracy of the orientation for both samples was within $\pm 5°$.

The measurements were performed with a MPMS-5XL superconducting quantum interference device (SQUID) using the extraction method. The dc magnetic field B was applied along $\langle 100\rangle$ or $\langle 110\rangle$, as was the drive ac field $B_{ac} = 0.4$ mT with frequency ranging from 0.1 to 1000 Hz. The measurements yield the dc magnetisation M as well as the real and imaginary components of the ac susceptibility, χ' and χ'' respectively. Three specific experimental protocols were adopted in order to investigate the influence of magnetic history:

- Zero-field-cooled scans (ZFC): the sample was brought to the temperature of interest in zero field and then the measurements were performed by increasing stepwise the magnetic field.
- Field-cooled cooling scans (FCC): the sample was brought to 70 K, a magnetic field was applied and the signal was recorded by decreasing stepwise the temperature.
- Field-cooled warming scans (FCW): the sample was brought to 70 K, and then cooled down to 5 K in a magnetic field. The signal was recorded by increasing the temperature stepwise.

All measurements have been performed once the sample has reached thermal equilibrium.

III. DC MAGNETISATION

Figure 1 displays the magnetic field dependence of the ZFC magnetisation M and its corresponding susceptibility $\Delta M/\Delta B$, deduced from numerical differentiation, for a set of temperatures between 5 and 50 K. The results are given for B along $\langle 100\rangle$, thus along the easy axis of the magnetic structure, in panels (a) and (b), and for B along $\langle 110\rangle$, in panels (c) and (d).

For both orientations, M increases almost linearly with B at low fields, which leads to a slowly varying $\Delta M/\Delta B$. By further increasing the magnetic field, a kink appears in the magnetisation curves, which is more clearly seen as a peak in the derivative $\Delta M/\Delta B$ and marks the transition from the helical to the conical phase at the critical field B_{c1}. For both sample orientations this peak is more pronounced at low temperatures and at 5 K it shifts to $\sim$40 mT in agreement with the B_{c1} values reported in the literature[12,14,19,27].

At high fields, M levels off above B_{c2} and reaches a temperature dependent value M_{sat}, which at 5 K amounts to $\sim$0.54 μ_B/Cu^{2+} for both sample orientations

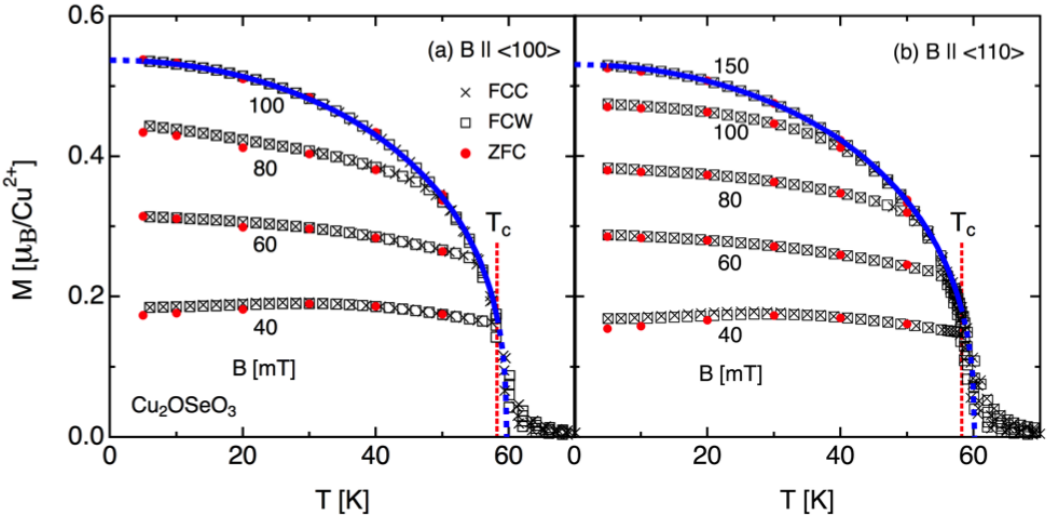

FIG. 2. Temperature dependence of FCC and FCW magnetisation of Cu_2OSeO_3 at several magnetic fields for (a) $B \parallel \langle 100 \rangle$ and (b) $B \parallel \langle 110 \rangle$. The ZFC data from M vs B measurements are included as well. The blue lines in both panels are fits of eq. 1 with the parameters given in the text. The red vertical dashed lines indicate $T_c = 58.2$ K.

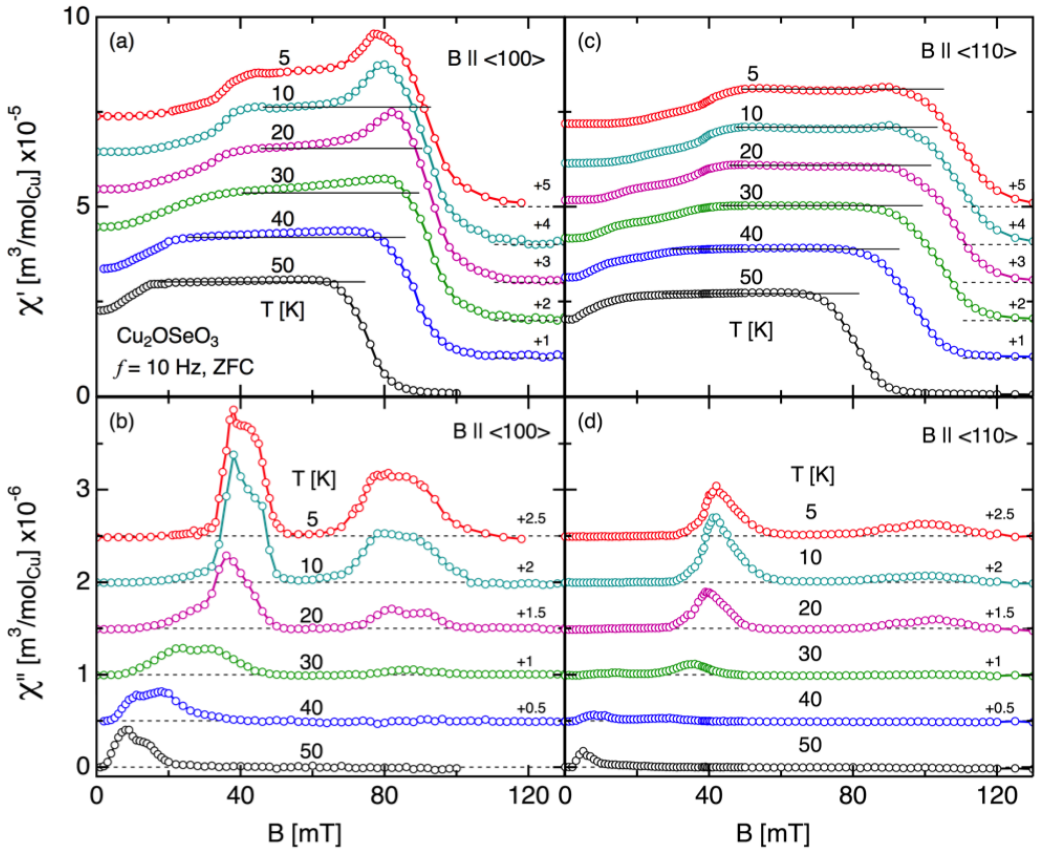

FIG. 3. Magnetic field dependence of ZFC χ' and χ'' of Cu_2OSeO_3 at selected temperatures from 5 to 50 K at $f = 10$ Hz. Panels (a) and (b) correspond to $B \parallel \langle 100 \rangle$ and panels (c) and (d) to $B \parallel \langle 110 \rangle$. The horizontal lines in panels (a) and (c) are guides to the eye. All curves have been shifted vertically with respect to the base line as indicated.

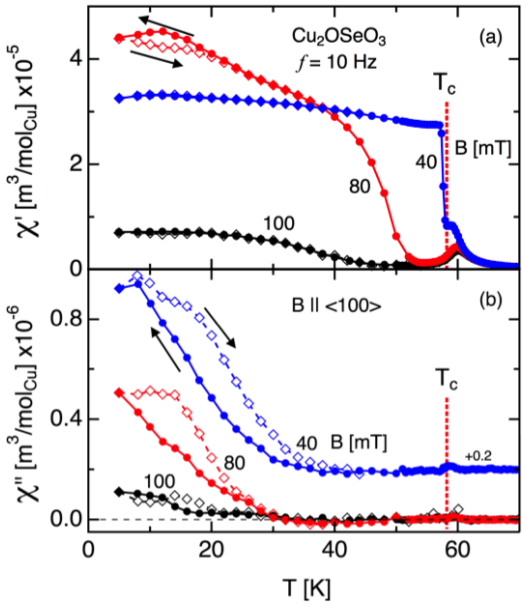

FIG. 4. Temperature dependence of FCC (solid markers) and FCW (open markers) χ' (a) and χ'' (b) of Cu_2OSeO_3 at various magnetic fields and $f = 10$ Hz for $B \parallel \langle 100 \rangle$. The vertical lines indicate $T_c = 58.2$ K. The χ'' curve for 40 mT has been shifted vertically with respect to the base line as indicated.

in agreement with literature[12–14,19,27]. However, the way M approaches M_{sat} below 20 K is very different for the two sample orientations. This is clearly seen in the deduced $\Delta M/\Delta B$ curves, where only for $B \parallel \langle 100 \rangle$ a maximum, centered at ∼80 mT for 5 K, develops close to B_{c2}. The observed behaviour and the differences between the two sample orientations follow the same trend as reported in the literature[14].

Figure 2 displays the temperature dependence of the FCC and FCW magnetisations for some specific magnetic fields with $B \parallel \langle 100 \rangle$ in panel (a) and $B \parallel \langle 110 \rangle$ in panel (b). The ZFC data from the M vs B curves are included as well. For both orientations, the ZFC magnetisation is slightly lower than the FCC and FCW ones, which practically overlap. For all magnetic fields the magnetisation increases monotonically with decreasing temperature with the exception of 40 mT, where for both orientations a broad maximum occurs around 30 K, that corresponds to B_{c1}. Close to T_c all data follow a generic curve that is reached at $B = 100$ mT for $B \parallel \langle 100 \rangle$ and beyond $B = 120$ mT, e.g. at 150 mT for $B \parallel \langle 110 \rangle$. The larger magnetic field value for $B \parallel \langle 110 \rangle$ should be attributed to the magnetocrystalline anisotropy. Deviations from these generic curves occur at temperatures and fields that correspond to the B_{c2} values determined from the inflection points of $\Delta M/\Delta B$ as derived from Fig. 1(b). For instance, for $B \parallel \langle 100 \rangle$ at 80 mT M deviates from the generic curve below ∼45 K, and this temperature shifts to higher values for lower magnetic fields.

These generic curves are the same for both sample orientations and can be accounted for by a modified power law[13] illustrated by the continuous lines in Fig. 2:

$$M_{sat}(T) = M_{sat}(0)\ \left[1 - \left(T/T_c^0\right)^n\right]^\beta \qquad (1)$$

with $M_{sat}(0) \approx 0.54\ \mu_B$/Cu, $n \approx 2$, $\beta \approx 0.38$ and $T_c^0 \approx 59.7$ K $\sim T_c + 1.5$ K. The exact values of the parameters are given in Table I and are in agreement with a previous study[13]. Close to T_c, Eq. 1 reduces to the simple power law (for $n = 1$) predicted theoretically[22], that mimics a 3D-Heisenberg behaviour.

IV. AC SUSCEPTIBILITY AT 10 Hz

Figure 3 illustrates the magnetic field dependence of ZFC χ' and χ'' at an intermediate frequency of $f = 10$ Hz for selected temperatures between 5 and 50 K. For both $B \parallel \langle 100 \rangle$ and $\langle 110 \rangle$ χ' increases slowly at low fields, similarly to dc susceptibility $\Delta M/\Delta B$. On the other hand, χ' in Figs. 3(a) and 3(c) does not show the peak at B_{c1} found in the $\Delta M/\Delta B$ curves, but a crossover to a plateau-like behaviour, characteristic of the conical phase. At 50 K, the plateau is very much horizontal for both field configurations, but at lower temperatures a slope sets in and below 30 K a peak develops at ∼ 80 mT, which is very weak for $B \parallel \langle 110 \rangle$ but well pronounced for $B \parallel \langle 100 \rangle$.

The corresponding χ'' is shown in Figs. 3(b) and 3(d) for both orientations. Around B_{c1}, for $B \parallel \langle 100 \rangle$, χ'' seems to consist of two adjacent peaks, which at 50 K are centred at 8 and 13 mT respectively. With decreasing temperature the amplitude of these peaks increases considerably and their positions move to higher magnetic fields. At 5 K they occur at 38 and 42 mT respectively. These two peaks are also observed for $B \parallel \langle 110 \rangle$ but with relatively weaker intensity and occur simultaneously only between 40 and 30 K. Above B_{c1} for both orientations, χ'' is zero in the conical phase, thus no dissipation is observed.

However close to B_{c2}, a broad maximum of χ'' appears below 30 K, which is hardly visible for $B \parallel \langle 110 \rangle$ but prominent for $B \parallel \langle 100 \rangle$, a configuration where the peak of χ' develops as well. Similarly to the peak of χ' for $B \parallel \langle 100 \rangle$, the maximum of χ'' increases with decreasing temperature. Such a peak in χ'' has not been observed in B20 magnets so far and seems to be a particularity of Cu_2OSeO_3.

The effect of thermal history is illustrated by Fig. 4, which depicts the temperature dependence of χ' and χ'' for FCC and FCW and $B \parallel \langle 100 \rangle$. A pronounced hysteresis is observed for χ'' at $B = 40$ mT below 40 K, which is hardly visible in χ' probably due to its weak temperature dependence in this temperature range. On the other hand, strong hysteresis appears in both χ' and χ'' at 80 mT below 30 K. At higher magnetic fields, e.g. 100 mT, both χ' and χ'' are much weaker and they hardly show any hysteresis.

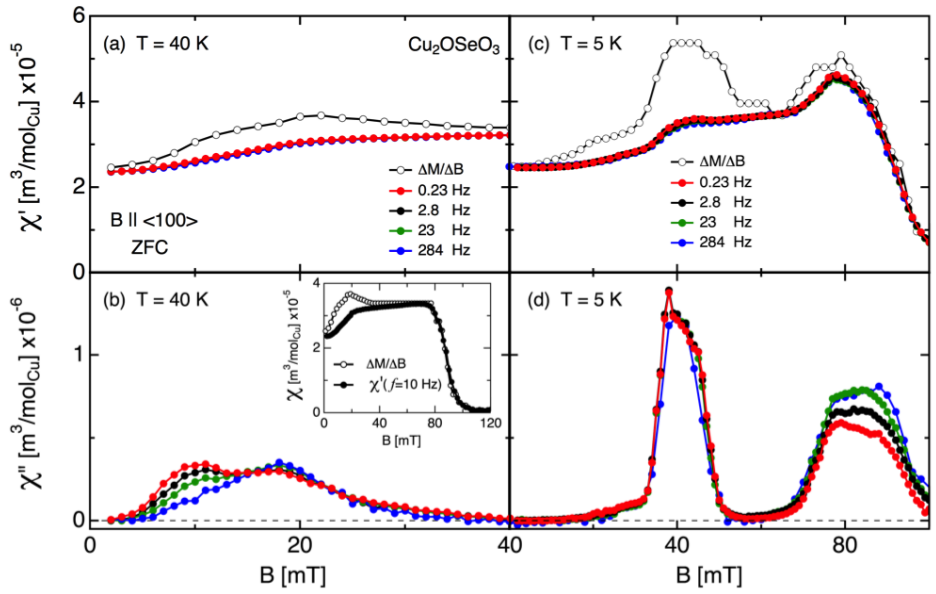

FIG. 5. ZFC χ' and χ'' as a function of magnetic field at various frequencies for 40 K in panels (a) and (b), and 5 K in panels (c) and (d) with $B \parallel \langle 100 \rangle$. The dc susceptibility $\Delta M/\Delta B$ from Fig. 1(b) is included as well and extends beyond B_{c2} up to 120 mT for 40 K in the inset of (b).

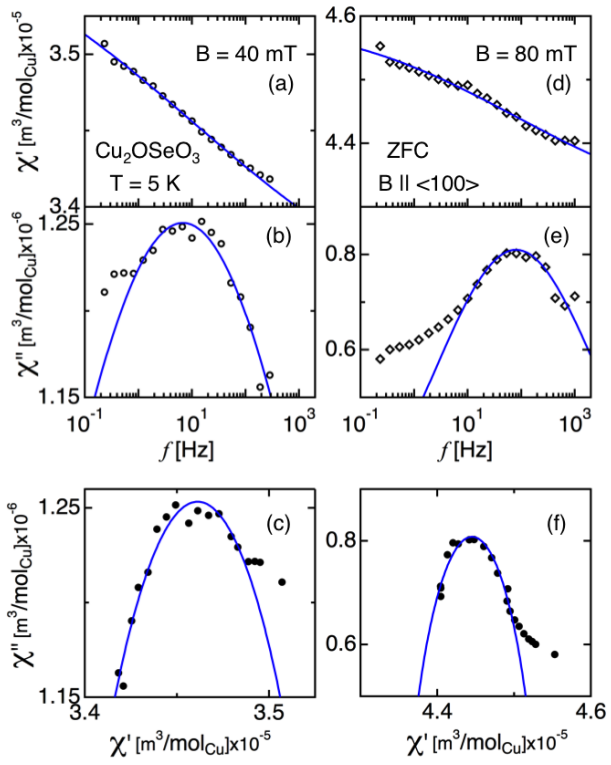

FIG. 6. Frequency dependence of χ' and χ'' at (a and b) 40 mT and (d and e) 80 mT for $B \parallel \langle 100 \rangle$. Panels (c) and (f) show χ'' plotted versus χ' for 40 and 80 mT respectively. The solid lines represent fits of the Cole-Cole formalism to the data.

V. FREQUENCY DEPENDENCE OF ZFC AC MAGNETIC SUSCEPTIBILITY

The relaxation phenomena associated with B_{c1} and B_{c2} presented in the previous section are most visible for $B \parallel \langle 100 \rangle$ and in the following we will focus on the results obtained in this orientation. Figure 5 displays the ZFC χ' and χ'' for various frequencies at 40 and 5 K. The figure highlights the differences between $\Delta M/\Delta B$ and χ' as $\Delta M/\Delta B$ develops a peak around B_{c1} while χ' shows a smooth crossover to a plateau. Above B_{c1}, the ac and dc susceptibilities converge for both temperatures and overlap close to B_{c2}.

The frequency dependence is more pronounced in χ'' in contrast to that of χ'. At 40 K, χ'' shows two peaks which are located at 10 and 18 mT, thus close to B_{c1}. Clear frequency dependence is observed in the amplitude of these peaks and is different for the two peak positions. The peak at 10 mT decreases with increasing frequency, while the one at 18 mT slightly increases. At 284 Hz only the peak at 18 mT is visible. On the other hand, at 5 K these two χ'' peaks seem to merge as shown in Fig. 5(d) and vary very weakly with frequency. In contrast, the broad peak in χ'', that appears close to B_{c2}, shows a noticeable frequency dependence.

A quantitative analysis of the frequency dependence of χ' and χ'' is provided by the modified Cole-Cole formalism[28,29]:

$$\chi(\omega) = \chi(\infty) + \frac{\chi(0) - \chi(\infty)}{1 + (i\omega\tau_0)^{1-\alpha}} \qquad (2)$$

with $\omega = 2\pi f$ the angular frequency, $\chi(0)$ and $\chi(\infty)$ the adiabatic and isothermal susceptibilities respectively and

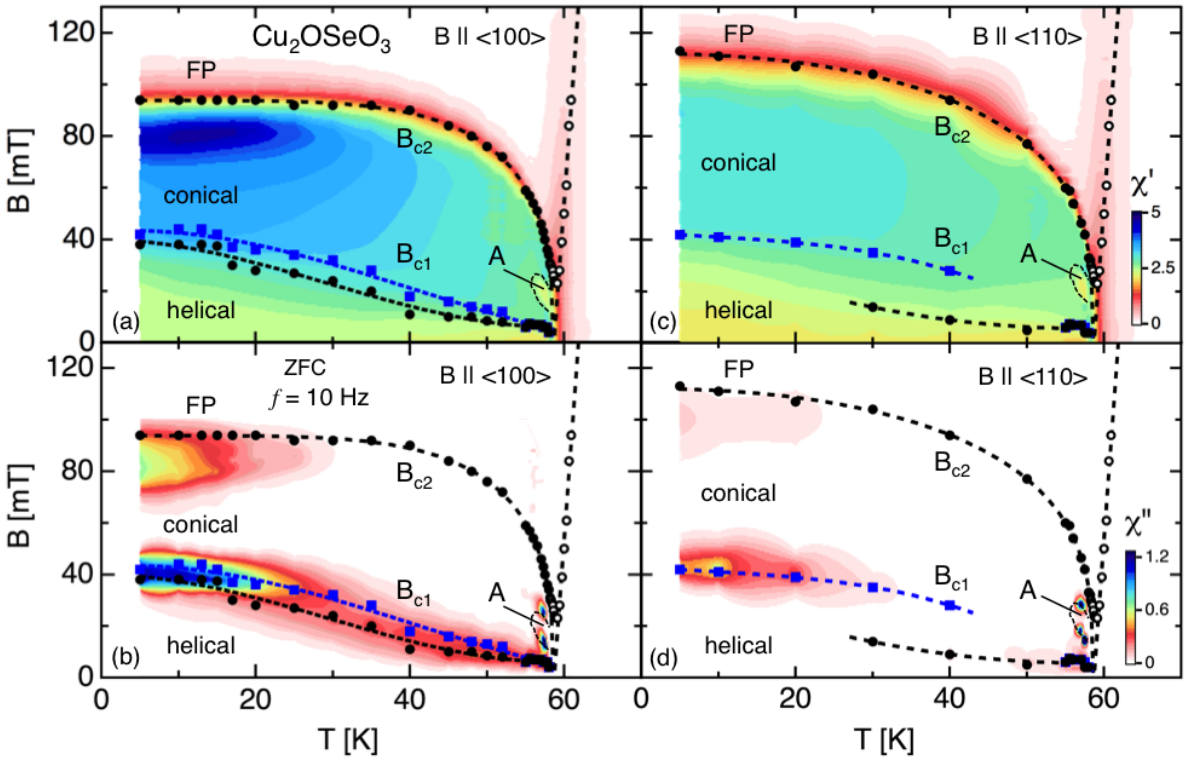

FIG. 7. Contour plots of χ' and χ'' displayed versus temperature and magnetic field at $f = 10$ Hz from ZFC measurements for $B \parallel \langle 100 \rangle$ in panel (a) and (b), and $B \parallel \langle 110 \rangle$ in panel (c) and (d). The phase boundaries B_{c1}, B_{A1}, B_{A2} and B_{c2} are shown as well. Below ∼50 K two B_{c1} lines are illustrated by the circles and squares at lower fields. In the contour plots, we identify the following phases: helical, conical, A for the A-phase and FP for the field polarised one. The units for χ' and χ'' are 10^{-5} and $10^{-6}\mathrm{m}^3/\mathrm{mol}_{\mathrm{Cu}}$ respectively.

$\tau_0 = 1/(2\pi f_0)$ the characteristic relaxation time with f_0 the characteristic frequency. The parameter α measures the distribution of characteristic relaxation times: $\alpha = 0$ corresponds to a single relaxation time, and $\alpha > 0$ to a distribution of relaxation times, which becomes broader as α approaches 1. Equation 2 leads to the in-phase and out-of-phase components of the susceptibility, and a relation between these two quantities discussed in our previous report[18].

Figure 6 illustrates the frequency dependence of ZFC χ' and χ'' at 5 K for 40 and 80 mT. With increasing frequency, χ' decreases very weakly, only by ∼3%, as seen in the panels (a) and (d). A more significant variation is found for χ'', which shows broad maxima at the characteristic frequencies $f_0 \sim 10$ Hz and 100 Hz for 40 and 80 mT, thus around B_{c1} and B_{c2} as seen in the panels (b) and (e), respectively.

The fit of eq. 2 to the data is illustrated by the solid lines in Fig. 6. It leads to $\alpha \sim 0.85$ and ~ 0.65 for B=40 and 80 mT, respectively, thus revealing the existence of broad distributions of relaxation times. In addition, deviations from the simple Cole-Cole behaviour are found at low frequencies, as illustrated in panels (b), (c), (e) and (f). These may originate from the co-existence of several relaxation processes similarly to what has been reported at B_{c1} close to T_c[18] and over a larger temperature and magnetic field range in $Fe_{1-x}Co_xSi$[30].

VI. DISCUSSION

The results presented in the previous sections reveal new features and qualitatively different phase diagrams for $B \parallel \langle 100 \rangle$ and $\langle 110 \rangle$. The magnetic phase diagrams are illustrated as contour plots in Fig. 7, which summarise the magnetic field and temperature dependence of the ZFC χ' and χ'' at $f = 10$ Hz for $B \parallel \langle 100 \rangle$ and $\langle 110 \rangle$ and include additional data close to T_c from our previous study[18]. The phase boundaries shown are determined following the same criteria as in our previous study[18]: B_{c1}, B_{A1} and B_{A2} from the peaks of χ'', and B_{c2} from the inflection points of χ' vs B.

We start the discussion with the behaviour of χ'' close to B_{c1}, which shows two adjacent peaks below ∼50 K, for $B \parallel \langle 100 \rangle$, as seen in Figs. 3(b), 5(b) and 5(d). These peaks result in two B_{c1} lines that merge into a single broad peak just below T_c, the frequency dependence of which bears the signature of more than one relaxation process[18]. On the other hand, the peaks of χ'' for $B \parallel \langle 110 \rangle$ lead to two discontinuous B_{c1} lines,

TABLE I. Parameters of the power law fits to the temperature dependence of M_{sat} and B_{c2} below $T_c = 58.2$ K for $B \parallel \langle 100 \rangle$ and $B \parallel \langle 110 \rangle$. For the sake of comparison the corresponding parameters from the literature are also provided.

	$M_{sat}(T)$			B_{c2}		
	$B \parallel \langle 100 \rangle$	$B \parallel \langle 110 \rangle$	Ref[13]	$B \parallel \langle 100 \rangle$	$B \parallel \langle 110 \rangle$	Ref[31]
$M_{sat}(0)$	0.54±0.01	0.53±0.01	0.559±0.007	–	–	–
$B_{c2}(0)$	–	–	–	94±2	112±1	85
$T_c^0 - T_c$	1.5±0.1	1.8±0.3	1.8±0.1	0.3±0.1	0.4±0.1	0
β	0.368±0.005	0.391±0.002	0.393±0.004	0.34±0.02	0.30±0.01	0.25
n	1.99±0.02	2.01±0.01	1.95	5.1±0.2	2.2±0.2	1

which coexist only at a limited temperature range, between ∼40 and ∼30 K, as seen in Fig. 3(d). This complex behaviour for both field orientations seems to be unique to Cu_2OSeO_3 and might be related to the two different Cu^{2+} sites, which might lead to slightly different magnetocrystalline anisotropies.

At high magnetic fields, a single B_{c2} line is found for each of the sample orientations. Close to T_c, the temperature dependence of B_{c2} is similar for both orientations but differences appear below ∼ 50 K: B_{c2} levels off with decreasing temperature for $B \parallel \langle 100 \rangle$, while it keeps increasing for $B \parallel \langle 110 \rangle$. The temperature dependences of the two B_{c2} lines can be accounted for by Eq. 1 and lead to the parameters given in Table I with $\beta \approx 0.32$ and $T_c^0 \approx 58.6$ K$\sim T_c + 0.4$ K for both orientations and different n: $n = 5.1 \pm 0.2$ for $B \parallel \langle 100 \rangle$ and $n = 2.2 \pm 0.2$ for $B \parallel \langle 110 \rangle$. These values deviate from those reported in the literature[31] and from those deduced from the temperature dependence of M_{sat}. On the other hand, close to T_c, both B_{c2} lines reduce to the same simple power law, for $n = 1$, that has been previously reported for the same samples[18].

Besides the different phase boundaries, the two sample orientations also lead to substantially different behaviour for both χ' and χ'' close to B_{c2} and below ∼30 K. The maxima that appear both in χ' and χ'' in this field and temperature range are marked for $B \parallel \langle 100 \rangle$, but are much weaker for $B \parallel \langle 110 \rangle$, as shown in Fig. 3. Similar differences are also found in the dc magnetisation as well as in previous reports[12–14]. Theory predicts a similar behaviour but with much more dramatic effects[22]. Indeed, while a continuous second order transition is expected when a magnetic field is applied outside the easy magnetisation axis, a discontinuous first order transition is predicted for $B \parallel \langle 100 \rangle$, i.e. when the magnetic field is applied along the easy magnetisation axis. This first order transition should appear as a jump of the magnetisation at $T = 0$ K, leading to a divergence of the derivative, thus of the susceptibility. According to theory the jump of the magnetisation at B_{c2} should be visible up to ∼50 K. In our measurements the maxima in χ' and $\Delta M/\Delta B$ appear only below 20 K. Thus, there is a limited agreement with theory at B_{c2}, which however, does not expand to B_{c1}, where theory predicts a single transition line and does not account for the two lines observed experimentally.

At this moment, we are not aware of any theory that could explain the significant dissipation phenomena that appear in χ'' and occur not only at B_{c1} but also at B_{c2} at low temperatures. In particular the strong χ'' at B_{c2} for $B \parallel \langle 100 \rangle$ has not been reported before neither for Cu_2OSeO_3 nor for other B20 chiral magnets and seems to be unique to Cu_2OSeO_3. A discussion on the origin of these effects can only be speculative based on our main observations that are the dependence on the sample orientation with respect to the magnetic field, the broad distributions of relaxation times seen in the values of α, the relatively long characteristic relaxation times τ_0 and the coexistence of several relaxation processes. Among these, the dependence on the sample orientation at B_{c2} might be related to the effects seen in the magnetisation curves and the theoretical predictions discussed in the previous paragraph.

The characteristic long relaxation times deduced from the Cole-Cole analysis close to B_{c1} and B_{c2} indicate rearrangements of large correlated volumes with extremely low associated energies of the order of $\hbar\omega$. In addition, it seems reasonable to assume that the distribution of relaxation times also reflects a distribution of volumes. It is not clear what the size of these volumes is and what delimits them, possibly defects, stress or frustration. These very slow relaxation phenomena might prevent the system from reaching thermodynamic equilibrium at low temperatures and thus explain the hysteresis between FCC and FCW data seen in Fig. 4.

VII. CONCLUSION

The dc magnetisation and ac susceptibility of Cu_2OSeO_3 reveal qualitatively different phase diagrams below 50 K depending on whether the magnetic field was applied along the easy $\langle 100 \rangle$ or the hard $\langle 110 \rangle$ crystallographic directions of the sample. The differences are not only in the specific values of the critical fields B_{c1} and B_{c2} but also in the behaviour of the magnetisation and susceptibility.

The B_{c1} transition from the helical to the conical phase splits in two well distinct lines below ∼50 K, which may be related to the two different Cu^{2+} sites. These two B_{c1} lines coexist only between 30 and 40 K for $B \parallel \langle 110 \rangle$, but expand almost over the whole temperature range for $B \parallel \langle 100 \rangle$.

Close to B_{c2}, the magnetisation and the susceptibility are in qualitative agreement with theory, which however foresees more dramatic effects with a discontinuous first order transition from the conical to the field polarised state when the magnetic field is applied along the easy axis and a continuous second order transition otherwise. In addition, below 30 K, an important χ'' signal appears close to B_{c2} for $B \parallel \langle 100 \rangle$, the origin of which is unclear. Similar dissipation phenomena have not been observed in Cu_2OSeO_3 or in other B20 magnets before.

At both B_{c1} and B_{c2} the frequency dependence of χ'' reflects the existence of very broad distributions of relaxation times and the superposition of several relaxation processes, which lead to thermal hysteresis and eventually prevent the system from reaching thermal equilibrium at low temperatures.

ACKNOWLEDGMENTS

The authors would like to thank G.R. Blake for checking the sample orientations and L.J. Bannenberg for fruitful discussions. F. Qian acknowledges financial support from the China Scholarship Council.

† Present Address: RM University of Twente, The Netherlands

[1] S. Mühlbauer, B. Binz, F. Jonietz, C. Pfleiderer, A. Rosch, A. Neubauer, R. Georgii, and P. Böni, Science **323**, 915 (2009).

[2] A. Tonomura, X. Yu, K. Yanagisawa, T. Matsuda, Y. Onose, N. Kanazawa, H. S. Park, and Y. Tokura, Nano Lett. **12**, 1673 (2012).

[3] X. Z. Yu, N. Kanazawa, Y. Onose, K. Kimoto, W. Z. Zhang, S. Ishiwata, Y. Matsui, and Y. Tokura, Nat Mater **10**, 106 (2010).

[4] W. Münzer, A. Neubauer, T. Adams, S. Muhlbauer, C. Franz, F. Jonietz, R. Georgii, P. Böni, B. Pedersen, M. Schmidt, A. Rosch, and C. Pfleiderer, Physical Review B **81**, 041203 (2010).

[5] X. Z. Yu, Y. Onose, N. Kanazawa, J. H. Park, J. H. Han, Y. Matsui, N. Nagaosa, and Y. Tokura, Nature **465**, 901 (2010).

[6] E. Moskvin, S. Grigoriev, V. Dyadkin, H. Eckerlebe, M. Baenitz, M. Schmidt, and H. Wilhelm, Physical Review Letters **110**, 077207 (2013).

[7] A. N. Bogdanov and D. A Yablonskii, Journal of Experimental and Theoretical Physics **68**, 101 (1989).

[8] A. N. Bogdanov and D. A. Yablonskii, Journal of Experimental and Theoretical Physics **69**, 142 (1989).

[9] A. Fert, V. Cros, and J. Sampaio, Nature Nanotechnology **8**, 152 (2013).

[10] J. S. White, K. Prša, P. Huang, A. A. Omrani, I. Živković, M. Bartkowiak, H. Berger, A. Magrez, J. L. Gavilano, G. Nagy, J. Zang, and H. M. Rønnow, Phys. Rev. Lett. **113**, 107203 (2014).

[11] S. Seki, X. Z. Yu, S. Ishiwata, and Y. Tokura, Science **336**, 198 (2012).

[12] T. Adams, A. Chacon, M. Wagner, A. Bauer, G. Brandl, B. Pedersen, H. Berger, P. Lemmens, and C. Pfleiderer, Phys. Rev. Lett. **108**, 237204 (2012).

[13] I. Živković, D. Pajić, T. Ivek, and H. Berger, Phys. Rev. B **85**, 224402 (2012).

[14] M. Belesi, I. Rousochatzakis, M. Abid, U. K. Rößler, H. Berger, and J. P. Ansermet, Phys. Rev. B **85**, 224413 (2012).

[15] S. Seki, J. H. Kim, D. S. Inosov, R. Georgii, B. Keimer, S. Ishiwata, and Y. Tokura, Phys. Rev. B **85**, 220406(R) (2012).

[16] A. A. Omrani, J. S. White, K. Prša, I. Živković, H. Berger, A. Magrez, Y.-H. Liu, J. H. Han, and H. M. Rønnow, Phys. Rev. B **89**, 064406 (2014).

[17] I. Levatić, V. Šurija, H. Berger, and I. Živković, Phys. Rev. B **90**, 224412 (2014).

[18] F. Qian, H. Wilhelm, A. Aqeel, T. T. M. Palstra, A. J. E. Lefering, E. H. Brück, and C. Pappas, Phys. Rev. B **94**, 064418 (2016).

[19] J.-W. Bos, C. V. Colin, and T. T. M. Palstra, Phys. Rev. B **78**, 094416 (2008).

[20] V. Dyadkin, K. Prša, S. V. Grigoriev, J. S. White, P. Huang, H. M. Rønnow, A. Magrez, C. D. Dewhurst, and D. Chernyshov, Physical Review B **89**, 140409 (2014).

[21] J. H. Yang, Z. L. Li, X. Z. Lu, M.-H. Whangbo, S.-H. Wei, X. G. Gong, and H. J. Xiang, Physical Review Letters **109**, 107203 (2012).

[22] O. Janson, I. Rousochatzakis, A. A. Tsirlin, M. Belesi, A. A. Leonov, U. K. Roessler, J. van den Brink, and H. Rosner, Nat Comms **5** (2014).

[23] J. Romhányi, J. van den Brink, and I. Rousochatzakis, Physical Review B **90**, 140404 (2014).

[24] P. Bak and M. Jensen, Journal of Physics C: Solid State Physics **13**, L881 (1980).

[25] A. Aqeel, J. Baas, G. R. Blake, and T. T. M. Palstra, unpublished (2016).

[26] K. H. Miller, X. S. Xu., H. Berger, E. S. Knowles, D. J. Arenas, M. W. Meisel, and D. B. Tanner, Phys. Rev. B **82**, 144107 (2010).

[27] C. L. Huang, K. F. Tseng, C. C. Chou, S. Mukherjee, J. L. Her, Y. H. Matsuda, K. Kindo, H. Berger, and H. D. Yang, Phys. Rev. B **83**, 052402 (2011).

[28] K. S. Cole and R. H. Cole, J. Chem. Phys. **9**, 341 (1941).

[29] D. Huser, A. J. van Duyneveldt, G. J. Nieuwenhuys, and J. A. Mydosh, J. Phys. C: Solid State Phys. **19**, 3697 (1986).

[30] L. J. Bannenberg, A. J. E. Lefering, K Kakurai, Y. Onose, Y. Endoh, Y Tokura, and C. Pappas, Phys. Rev. B **94**, 134433 (2016).

[31] I. Levatić, P. Popčević, V. Šurija, A. Kruchkov, H. Berger, A. Magrez, J. S. White, H. M. Rønnow, and I. Živković, Sci. Rep. **6**, 21347 (2016).